AFRL-SR-AR-TR-07-0456

# REPORT DOCUMENTATION PAGE



| 1. AGENCY USE ONLY *(Leave blank)* | 2. REPORT DATE | 3. REPORT TYPE AND DATES COVERED |
|---|---|---|
| | April 30, 2007 | Final Progress Report |

**4. TITLE AND SUBTITLE**

Spin-based lattice gas quantum optics in solids using optical addressing

**5. FUNDING NUMBERS**

Grant#: F49620-01-1-0566

**6. AUTHORS**

Marlan O. Scully, Olga Kocharovskaya, George Welch,
Philip Hemmer, M. Suhail Zubairy, Goong Chen

**7. PERFORMING ORGANIZATION NAME(S) AND ADDRESS(ES)**

Texas Engineering Experiment Station (TEES)
332 Wisenbaker Bldg. MS 3000
College Station, Texas 77843-3000

**8. PERFORMING ORGANIZATION REPORT NUMBER**

**9. SPONSORING/MONITORING AGENCY NAME(S) AND ADDRESS(ES)**

Air Force Office of Scientific Research
875 North Randolph Street, Suite 325
Arlington, VA 22203

Dr Gernot Pomrenke/NE

**10. SPONSORING/MONITORING AGENCY REPORT NUMBER**

Award #: F49620-01-1-0566

**11. SUPPLEMENTARY NOTES**

**12a. DISTRIBUTION/AVAILABILITY STATEMENT**

Distribution Statement A unlimited

**12b. DISTRIBUTION CODE**

**13. ABSTRACT** *(Maximum 200 words)*

The purpose of this project was to develop quantum computing hardware suitable for implementing quantum lattice-gas algorithms, with eventual application to turbulent flow simulations. A number of quantum systems were investigated, including rare-earth dopants in oxide crystals and in II-VI semiconductors. However, in the option year it was decided to concentrate exclusively on nitrogen-vacancy (NV) color centers in diamond. Surprising, it was found that NV diamond exhibited the key elements needed to develop few-qubit room-temperature solid-state quantum processing nodes. This included the ability to optically initialize and readout the NV electron spin state, fractional millisecond lifetimes for electron spins, and few-nanosecond electron spin Rabi flops. We also demonstrated the relatively long distance (few nanometer) coupling of a single NV spin to the electron spin of a single substitutional nitrogen (N). To achieve long range optical interconnections and entanglement between nodes, cryogenic cooling will likely still be required to sufficiently narrow the optical absorption lines. To this end we located diamond samples with unusually high purity, and found NV centers in these crystals that exhibited exceptionally narrowband and stable optical lines. We also demonstrated electric field tuning of the optical transition frequency as required for controlling atom-atom and atom-cavity coupling.

**14. SUBJECT TERMS**

Quantum coherence, quantum optics, lasers

**15. NUMBER OF PAGES**

53

**16. PRICE CODE**

| 17. SECURITY CLASSIFICATION OF REPORT | 18. SECURITY CLASSIFICATION OF THIS PAGE | 19. SECURITY CLASSIFICATION OF ABSTRACT | 20. LIMITATION OF ABSTRACT |
|---|---|---|---|
| UNCLASSIFIED unclassified | UNCLASSIFIED Unclassified | UNCLASSIFIED Unclassified | SAR ( same as report) Unclassifed |

# Final report F49620-01-1-0566: Spin-based lattice-gas quantum computers in solids using optical addressing

**Executive summary:**

The purpose of this project was to develop quantum computing hardware suitable for implementing quantum lattice-gas algorithms. Such algorithms require large arrays of few-qubit quantum processing nodes, where the nodes are inter-connected using only near-neighbor coupling. Requirements for qubit coherence lifetime in a lattice-gas computer are also less stringent as lattice-gas simulations are often designed to only simulate the average properties of a large ensemble. The motivation for this approach is that it will allow large, many-qubit quantum computers to be developed without solving the challenging problem of global, long-time entanglement. Moreover these large quantum arrays will be immediately applicable to challenging problems such as turbulent flow simulations.

This project involved a large-scale international collaboration, and several promising approaches were investigated. The common requirements were that the qubits be quantum states of long-lived spin systems in solids, and that they be optically addressable for both initialization and readout. Of the systems investigated, the most promising were rare-earth doped oxide crystals, especially Pr and Eu doped $Y_2SiO_5$ (YSO), and nitrogen-vacancy (NV) color centers in diamond. Pr and Eu doped YSO showed the most early promise in the form of half minute coherence times with microsecond single-qubit gate operations, and long-range (~100 nm) two-qubit gates between nearby spins. However, in the option year the decision was made to concentrate exclusively on NV diamond due to the fact that single NV spins can easily be addressed, whereas Pr and Eu:YSO are currently restricted to ensembles.

Once the decision was made to concentrate on NV diamond, rapid progress was made. Surprising, it was found that NV diamond exhibited the key elements needed to develop few-qubit room-temperature solid-state quantum processing nodes. These included the ability to optically initialize and readout the NV electron spin state, fractional millisecond lifetimes for electron spins, and few-nanosecond electron spin Rabi flops. We also demonstrated the relatively long distance (few nanometer) coupling of a single NV spin to the electron spin of a single substitutional nitrogen (N).

To achieve long range optical interconnections and entanglement between nodes, cryogenic cooling will still be required to sufficiently narrow the optical absorption lines. In addition, long distance entanglement requires stable, but tunable optical lines. We therefore demonstrated electric field tuning of the optical transition frequency, found diamond samples that exhibited exceptionally stable optical lines, and also mapped out the excited state energy level structure of the NV center. We found that it is possible to simultaneously excite optical Raman transitions on one excited state branch, while using a cycling transition on the other for readout.

## 1. Review of two-qubit quantum logic in ensembles of Eu doped $Y_2SiO_5$.

The first scalable quantum logic demonstration in an optically addressed solid was performed by Australian National University subcontractors, Manson and Sellars. The material chosen for the demonstration was Eu doped $Y_2SiO_5$ (Eu:YSO). It was selected because of the long coherence time of the optical $^7F_0$ to $^5D_0$ transition associated with the $Eu^{3+}$ ions at 579 nm. Below 4K the coherence time is 2.6 ms, which is approaching the lifetime limit. This long coherence time simplifies the implementation of the optical pulse sequences needed to control the gate operations by allowing them to be generated by simply modulating a continuous wave laser with acousto-optic shutters.

The dominant interaction between the Eu ions is a non-resonant electric dipole-dipole interaction. The $Eu^{3+}$ dopant ion possesses a permanent electric dipole moment that depends on the electronic state of the ion and hence, exhibits a linear Stark shift. The dipolar interaction between two ions is a consequence of the electric dipole of one ion inducing a Stark shift in the other. Of main interest in implementing two qubit gate operations is the small change in the interaction when the first ion is excited out of the $^7F_0$ ground state into the $^5D_0$ excited state. In the following unless explicitly stated otherwise we will refer to the changing component of the dipolar interaction as simply the electric dipolar interaction. Having said this, the large unchanging component of the dipolar interaction is a major source of inhomogenous broadening in the optical transitions and as will be discussed later has significant implications in scaling to more than two qubits. The strength of the electric dipolar interaction between two ions can be determined from the linear Stark shift in the optical transition, estimated to be 35kHz/V-cm$^{-1}$, and the relative position of the ions. For Eu ions in adjoining Y sites, separated by 0.5 nm, the interaction is expected to be of the order of 10 GHz. The dipolar interaction falls off at the inverse of the cube of the separation between the ions so at 10 nm the interaction strength reduces to 10 MHz. The interaction is also angular dependent so reflecting the position of one ion about a plane perpendicular the dipole moment of the second will reverse the sign of the interaction.

The challenge in implementing quantum logic in rare earth doped crystals is due to a combination of two factors: the weak oscillator strength of the optical transitions, and inhomogeneity in the crystal. In a Eu doped YSO crystal the Eu ions substitute for the Y ions in the lattice and are distributed randomly throughout the available sites in the sample. In general, each of these ions has a unique optical transition frequency that is determined by the local crystal environment (i.e. inhomogeneous broadening). Therefore, in principle, coherent transitions can be driven between the ground and excited states of any desired Eu ion by exciting with a sufficiently narrowband optical laser. In practice, the Eu optical transition is too weak to allow optical detection of an individual ion. Therefore to increase signal strength, many dopant ions are incorporated into the crystal. In fact, so many dopant ions are used that even a narrowband laser excites an ensemble, rather than a single ion. However, by precise optical preparation of the ensemble initial state, we can select a well-defined subset that consists of essentially identical ions. Although we use ensembles, the ability to place every atom in an identical initial state enables this demonstration to be performed without the mostly-classical pseudo-vectors that were used in liquid NMR quantum computers.

The basic techniques used to prepare the ensemble were developed by Pryde et al.[1] to enable the study of ion-ion interactions. In their paper they also proposed the use of these techniques for quantum computing applications in rare earth doped materials and demonstrated single qubit operations. The general concept is to use optical pumping to select out a subgroup of ions with the desired characteristics. In principle any characteristic, which is spectroscopically resolvable, can be selected. Briefly, this is accomplished by applying a sequence of optical pulses that have no net effect on ions with the exactly the desired properties. However, ions whose spectral properties deviate from that of the ideal case are optically pumped away (i.e. their absorption is bleached out so that they will not interact with the exciting laser during the subsequent experiment). As an example of using such a preparation pulse sequence to create an ensemble of identical ions, consider Figure 1. Here, a hole is first burned into the broad inhomogeneous optical linewidth of the dopant ion transition. The hole width is usually chosen to be in the range of 1MHz, so that it will be transparent to optical pulses having a smaller bandwidth. Ultimately, this pass-bandwidth essentially defines the limiting logic gate speed, which would be on the order of 1 microsecond in this case. In the center of this broad spectral hole, a narrow anti-hole is then created. This is done by using a narrowband laser to selectively excite a transition from one of the other ground-state ion sublevels to a convenient excited state, thereby optically pumping a narrowband spectral ensemble of the ions back. The width of this narrow anti-hole is determined by the inhomogeneous width of the spin transition, which is on the order of 100 kHz.

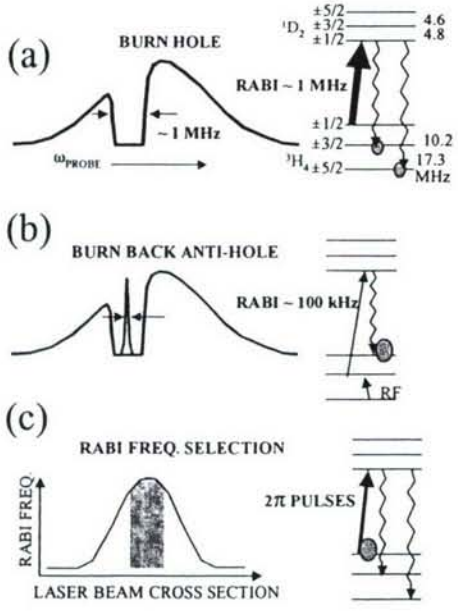


**Figure 1. Pulse preparation sequence for distilling an ensemble of ions with well-defined properties out of an initially inhomogeneous distribution. (a) First a broad hole is burned via spectral hole**

[1] "Solid State Coherent Transient Measurements Using Hard Optical Pulses," G. J. Pryde, M. J. Sellars, and N. B. Manson, *Phys Rev Lett* **84**, 1152, (2000).

**burning. (b) Next a narrow anti-hole is created in the center of the broad hole using optical pumping with a narrowband laser. (c) Finally, a subset of ions with well-defined interaction strengths is selected using a series of $2\pi$ pulses to bleach out ions that do not have the correct interaction strength.**

In principle, all the ions in this narrow anti-hole will respond in the same way to a sufficiently short laser pulse. However, in practice, non-uniformities in the laser intensity and the local crystal environment cause each ion to respond at a different rate (Rabi frequency) to an applied laser pulse. To overcome this limitation, a series of $2\pi$ laser pulses are applied that are designed to leave most of the ions in the ground state. Any ion that does not respond with the correct Rabi frequency is left partially excited and is optically pumped away after a few cycles. When driven with sufficiently short pulses (less than 10 μs), the remaining ions can be viewed as an ensemble of identical single qubits.

For long periods of evolution, $\pi$ pulses are needed to rephase the ensemble, because the remaining 100 kHz inhomogeneous broadening means that the optical coherence will eventually dephase. This rephrased coherence, or optical echo, is also useful for quantum state readout because it produces a measurable optical output beam whose properties are completely determined by the quantum state of the ensemble. The optical echo output also has the practical advantage that it is time delayed relative to any of the excitation laser pulses, so that there is no interference between input and output signals. As an example of photon echo readout of the time evolution of an ensemble of ions, Figure 2 shows a series of two-pulse photon echo sequences applied to an optically prepared ensemble. Each sequence consists of an initial pulse of varying length placing the ensemble in a coherent superposition state, while the second pulse is a fixed $\pi$ pulse used to rephase the coherence, which then is observed as a photon echo. As the length of the first pulse is increased the Rabi nutation in the echo amplitude is clearly visible. Here, only the in-phase part of the echo amplitude is plotted to illustrate the ability of the experimental setup to perform phase sensitive measurements.[2] The quadrature part is small as expected.

To perform a 2-qubit operation, two of the anti-holes described above where created inside a single wide spectral hole, with one anti-hole used as the target qubit and the second used as the control. The interaction between the target and control ions can be observed using a technique known as echo demolition. Here, a two-pulse photon echo sequence is first applied to the target ensemble. This consists of the usual $\pi/2$ pulse followed after a delay by the rephasing $\pi$ pulse. For echo demolition, a perturbing pulse is applied to the control ensemble at the same time as the rephasing pulse is applied to the target. The effect of the perturbing pulse is to excite the control ions which then impart a Stark frequency shift, and hence a phase shift, to each of the ions in the target ensemble. Since the perturbation is only applied during rephasing part of the echo sequence, its effect is not cancelled as would be the case if it were applied immediately after the initial pulse.

---

[2] "Experimental demonstration of quantum state tomography applied to dopant ions in a solid," J. J. Longdell and M. J. Sellars, **quant-ph/0208182.**

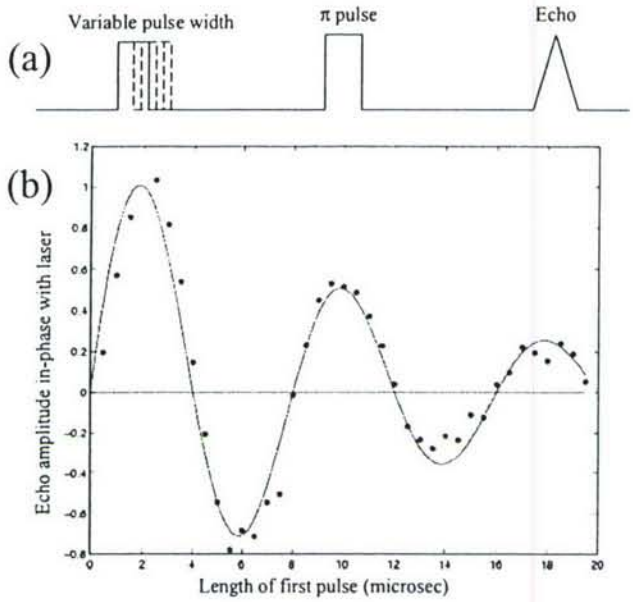


**Figure 2. Observation of Rabi nutation (single qubit rotations) using photon echo readout. (a) The pulse sequence with a variable initial pulse width. (b) The corresponding echo signals vs first pulse width. To illustrate phase sensitivity, only the in-phase part of the signal is shown. The quadrature part is small, as expected. To achieve such high contrast, 10 2π pulses were applied to prepare the ensemble, as described earlier.**

Given the random doping of the control (and target) Eu ions, the distribution of optical frequency shifts experienced by the target ions will be random, centered about zero. As a result the perturbing pulse will reduce the echo amplitude. This is shown in Figure 3, where the increasing time interval between pulses in the echo sequence also corresponds to a longer perturbation time. As shown, when there is no perturbation (+ symbols), the echo amplitude decays as expected for the coherence time ($T_2$) of the optical transition. However, when the perturbation is applied (square symbols) the echo amplitude is substantially reduced. Note that the vertical axis is a log scale, so that the echo amplitude reduction is large. The echo demolition caused by the perturbing pulse as a function of the delay between pulses, and hence as a function of the accumulated phase shift, is a measure of the distribution of frequency shifts induced on the target ion by optically exciting the control ion. When the perturbation is applied immediately after the first pulse (circle symbols), its effect is cancelled by the rephrasing pulse, as expected. The residual decrease in echo amplitude in this data is due to random-time excited-state population decay of the control atoms.

The dependence of the echo amplitude on the timing of the control ion perturbation pulse confirms that the observed echo reduction is due to induced frequency shifts. By comparing the first two series the distribution was found to be a Lorentzian centered about zero with a FWHM of 500 Hz. The FWHM shift represents a shift of 0.5% of the 100kHz width of the anti-holes. The small observed shifts reflect the low density of the ions that make up the control qubit, approximately 1 ion per 100 x 100 x 100 $nm^3$.

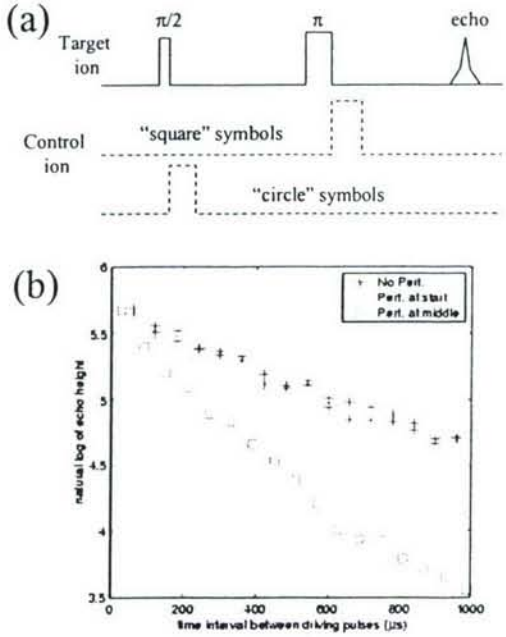


**Figure 3. (a) Target and control ion pulse sequences for echo demolition. (b) Echo demolition vs perturbation time (square symbols). Since the echo amplitude decays with increasing delays even in the absence of a perturbation, the "plus" symbols show this for comparison. Note the amplitude is a log scale so that the echo demolition significantly reduces the echo amplitude. In addition, the echo amplitude is also reduced due to random-time decay of the control-ion excited-state. This is shown by the "circle" symbols, which correspond to the control ion being optically excited during the entire echo pulse sequence so that its perturbative effects should be cancelled by rephrasing, but are not perfectly cancelled because some of the control ions decay the echo is observed.**

To be useful for quantum logic, the echo demolition must be modified to remove the randomness of the perturbation, so that it becomes a controlled phase shift that does not decrease the echo magnitude. This is accomplished by using spectral hole burning along with the dipole coupling-induced Stark frequency shift itself to further prepare the target ensemble. More precisely, the control ions are optically excited and the target ions that do not shift in frequency by the correct amount are optically pumped away. Conceptually this technique has been previously proposed.[3] The problem is that the number of suitable ions depends on the volume of the spherical, or other shape, shell which in turn is proportional to the distance. Therefore, to ensure that a significant fraction of the target ions have the appropriate control ion, the ion-ion separation must be relatively large, ~ 100 nm. Failing to do this results in only a small fraction of the initial target ion ensemble having the correct coupling to its respective control ion. This causes a substantial signal to noise penalty that becomes exponentially worse as the number of coupled qubits increases, in analogy with the situation in liquid NMR. On the other hand, the use of a large ion-ion separation means that the conditional frequency shift is small,

[3] "Quantum computer hardware based on rare-earth-ion-doped inorganic crystals," Nicklas Ohlsson, R. Krishna Mohan, Stefan Kroll, *Opt. Comm.* **209**, 71 (2002).

due to the inverse cubic distance dependence. In practice, to achieve an acceptably small signal-to-noise penalty, the coupling induced frequency shift is actually smaller than the width of the anti-hole that is used to define the target ion ensemble. Thus, the correct sub-ensemble cannot be selected using straightforward hole burning techniques.

To solve this state-preparation problem, echo-based techniques are borrowed from microwave NMR spectroscopy. Specifically, an echo pulse sequence is constructed that returns a target ion, with the correct control ion interaction, to its starting point in the ground. However, target ions with no control ion or with a control ion coupling of the wrong strength is not returned completely to its ground state, and is therefore optically pumped away after several cycles. This is illustrated in Figure 4. The spectral resolution of this technique is limited by the optical coherence time, which is orders of magnitude narrower than the width of a typical anti-hole.

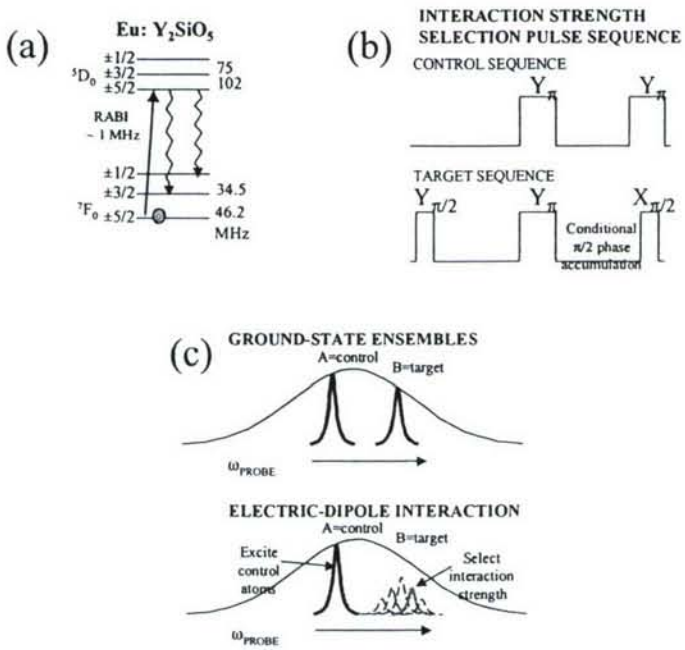


**Figure 4. (a) Simplified level diagram of Eu doped $Y_2SiO_5$ (Eu:YSO). (b) Pulse sequence for state selection based on control-target interaction strength. (c) Diagram illustrating effects of interaction strength selection pulses.**

The operation of the resulting conditional quantum phase gate is shown in Figure 5. Here the in-phase and quadrature parts of the echo signal are plotted (superimposed) in Figure 5(a) as a function of time. Clearly, when the control ion is excited, the echo is phase shifted. Significantly, the echo magnitude is essentially the same in both cases, when in-phase and quadrature parts are properly summed (see Figure 5(b)), as required for high fidelity quantum logic. Thus, the echo is no longer demolished by the perturbing pulse, but instead experiences a conditional phase shift (i.e. conditional quantum phase gate). The phase shift in this data is about 20 degrees, but in principle can be made larger

by further refinement of the state preparation process, and upgrade of the experimental setup.

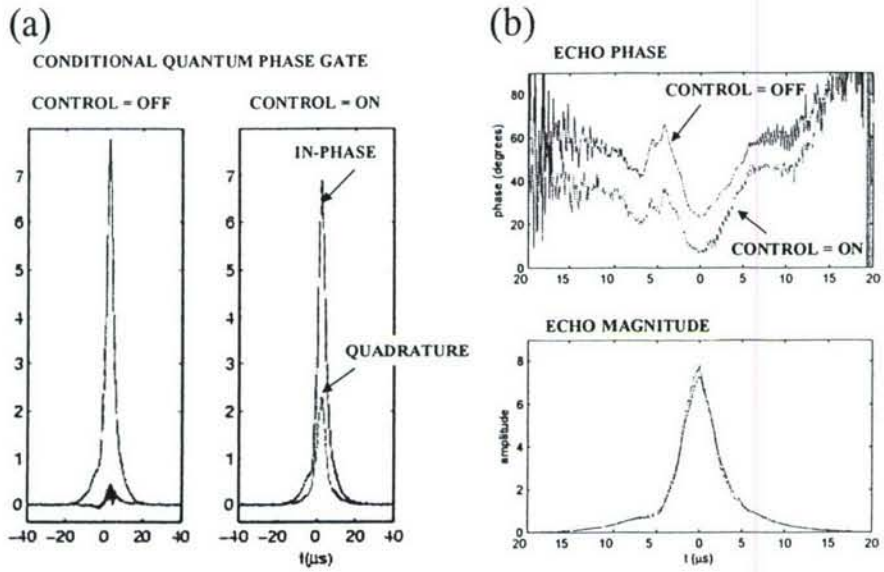


**Figure 5. Conditional quantum phase gate demonstration. (a) The phase-gate data for in-phase and quadrature echo signals are shown without (left) and with (right) the control ion excited. (b) The phase gate date for echo magnitude and phase. Significantly the phase shift is produced without noticeable decay in the echo magnitude, given by the rms sum of in-phase and quadrature signals. To achieve such a clean demonstration in the presence of control atom decay, the control ions were actually excited in both cases, but in the case labeled "CONTROL = OFF" they were excited during the entire echo sequence, so that the perturbation was cancelled by rephasing. The phase shift in this very first experiment is about 20-degrees, but in principle can be made larger than $\pi$ by upgrading the experiment.**

## 2. Half minute coherence lifetime in a solid.

The first demonstration of an ultra-long coherence lifetime in a solid was performed by Australian National University subcontractors, Manson and Sellars. The material chosen for the demonstration was Pr doped $Y_2SiO_5$ (Pr:YSO). It was selected because of its relatively long ground state spin coherence time, ~0.5 msec and its relatively strong optical transition strength, compared to Eu:YSO. The strong oscillator strength ($3 \times 10^{-7}$) allows nearly 100% absorption of a resonant laser beam. Combining this with the ability to manipulate spins optically, creates the potential for long range quantum entanglement by transferring quantum information from photons to spins.

The key to lengthening the spin coherence lifetime in Pr:YSO is to turn-off interactions with other spins in the host crystal. To see how this might be accomplished, consider the simplified spin sub-level diagram of Pr:YSO shown in Figure 6(a). When a magnetic field is applied, the Kramer's degenerate spin sublevels split due to the Zeeman effect. Here, the effect of an axial magnetic field (along the ion quantization axis) is illustrated. Owing to the zero-field sublevel splitting, many of the spin levels show a crossing at some magnetic field strength. This happens in all systems with spin 1 or greater. Pr:YSO has spin 7/2 and so has many such crossings. In practice, most of these crossing are avoided (ie anti-crossings). Near an anti-crossing, the spin sublevels have a quadratic energy dependence on the magnetic field strength. This means that there is no longer a linear Zeeman shift and the energy levels are much less sensitive to small changes in the applied magnetic field. Thus fluctuations in the local magnetic field at the Pr ion due to other spins in the host do not cause large frequency shifts, and hence the spin coherence lifetime is increased.

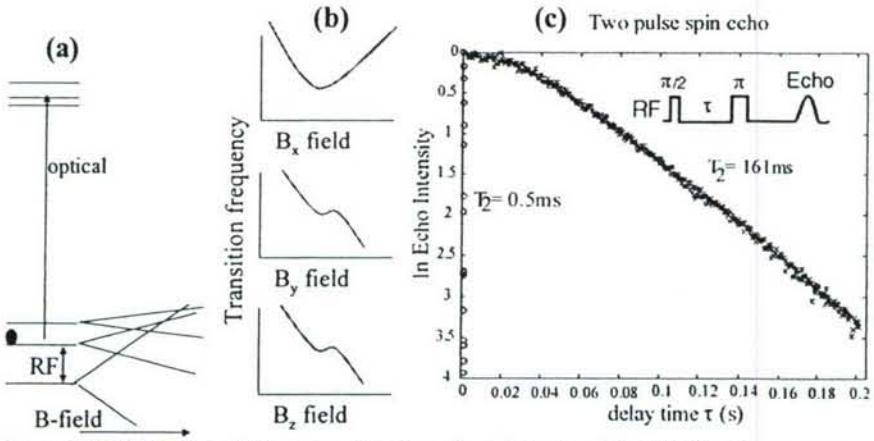


**Figure 6. (a) Splitting of the ground-state spin sublevels of Pr:YSO in the presence of an axial magnetic field, showing level crossings. (b) In practice, level crossings are usually avoided resulting in a quadratic dependence of energy level on applied magnetic field strength. In a system such as Pr:YSO, it is possible to find level anti-crossings that give 3-D magnetic field insensitivity. (c) Near a 3-D anti-crossing, the spin lifetime can increase by more than two orders of magnitude.**

The situation is actually more complex than this because the magnetic field is a vector quantity. As a result, the magnetic insensitivity may only apply to one or two directions of the applied magnetic field, so that fluctuations of the magnetic field in other directions might still produce linear Zeeman shifts and hence shorten coherence times.

Fortunately for Pr:YSO it is possible to find level anti-crossings that show quadratic Zeeman shifts along all three magnetic field axes, as illustrated in Figure 6(b).

To find these 3-D anti-crossings it is necessary to first simulate the Pr:YSO magnetic interaction. This is done by starting with the spin Hamiltonian given by:[4]

$$H = \vec{B}\cdot\left(g_J^2\mu_B^2\ddot{\Lambda}\right)\cdot\vec{B} + \vec{B}\cdot\left(\gamma_N\ddot{E} + 2A_J g_J \mu_B \ddot{\Lambda}\right)\cdot\vec{I} + \vec{I}\cdot\left(A_J^2\ddot{\Lambda} + \ddot{T}_Q\right)\cdot\vec{I}$$

where the $\ddot{\Lambda}$ tensor is given by

$$\Lambda_{\alpha\beta} = \sum_{n=1}^{2J+1}\frac{\langle 0|J_\alpha|n\rangle\langle n|J_\beta|0\rangle}{\Delta E_{n,0}}$$

$\ddot{E}$ is the 3 X 3 identity matrix, $\vec{B}$ is the magnetic field, and $\vec{I}$ is the nuclear spin vector, $g_J$ is the Lande $g$, $\gamma_N$ is the nuclear gyromagnetic ratio, $A_J$ is the hyperfine interaction. The term $\vec{I}\cdot\ddot{T}_Q\cdot\vec{I}$ described the nuclear electric quadrupole interaction and $A_J^2\vec{I}\cdot\ddot{\Lambda}\cdot\vec{I}$ is the second order magnetic hyperfine or pseudoquadrupole interaction. Next, many anti-crossings are explored for a variety of magnetic field strengths and directions until one with a 3-D quadratic Zeeman shift is found.

Once a suitable magnetic field direction and magnitude has been determined, an experiment can be performed. The result is shown in Figure 6(c).[5] As can be seen the spin coherence lifetime can be lengthened by more than 2 orders of magnitude. More importantly, the residual spin decoherence was found to decay as a quadratic exponential in time, meaning it decays as exp(-(t/τ)2). This is critical because most quantum error correction schemes require the short-time decay to be slower than the linear exponential decay that is usually assumed.

One quantum error correction scheme in particular has shown great promise to extend the spin decoherence time. This is the so-called "bang-bang" error correction protocol, and it involves applying a series of pi pulses to reverse and therefore cancel decoherence, in analogy to spin echoes. However, unlike the usual spin echo the pi-pulses in the bang-bang scheme must be repeated on a time scale short compared to the dephasing time, i.e. before significant errors can accumulate. Applying this technique to Pr:YSO at the anti-crossing resulted in a coherence time of 21 seconds, nearly half a minute, see Figure 7.[6] This is nearly 50,000 times the intrinsic dephasing time of 0.5 msec. For the typical 1 microsec gate time in this material, this translates to $10^7$ single qubit gate operations per coherence lifetime.

---

[4] J. J. Longdell, M. J. Sellars, and N. B. Manson, "Hyperfine interaction in ground and excited states of praseodymium-doped yttrium orthosilicate," PHYSICAL REVIEW B 66, 035101 2002

[5] Fraval E, Sellars MJ, Longdell JJ, "Method of extending hyperfine coherence times in Pr3+: Y2SiO5," PHYSICAL REVIEW LETTERS 92 (7): Art. No. 077601 FEB 20 2004

[6] Fraval E, Sellars MJ, Longdell JJ, "Dynamic decoherence control of a solid-state nuclear-quadrupole qubit," PHYSICAL REVIEW LETTERS 95 (3): Art. No. 030506 JUL 15 2005

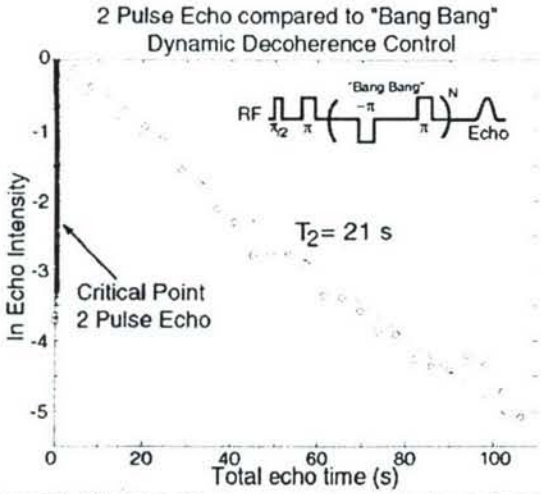


**Figure 7. The bang-bang error correction is used to extend the spin coherence time of Pr:YSO out to almost half minute. Here up to 25,000 rephasing pulse sequences were used with ~2 ms between pi pulses.**

## 3. Room-temperature spin qubits in nitrogen-vacancy (NV) diamond.

Optically active nitrogen-vacancy (NV) defects in diamond have attracted increasing attention for quantum optical applications following the discovery that the spin states of individual centers can be determined using confocal microscopy. The structure of the NV colour center is shown in Figure 8(a). It consists of nitrogen and a vacancy in an adjacent lattice site. The NV defect is negatively charged and has an electron spin triplet (S=1) ground state.[7] The transition between ground and excited spins triplets has a large oscillator strength (0.12), which allows the optical detection of single NV defects.

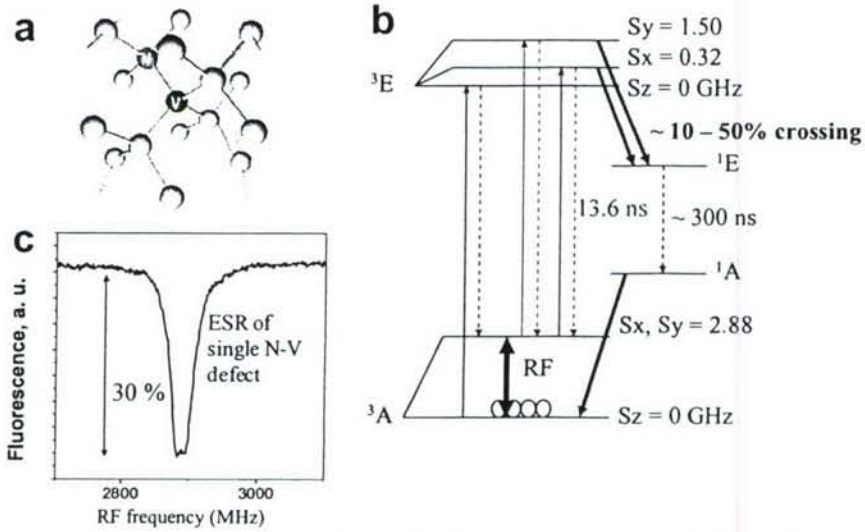


**Figure 8. Structure, energy levels and coherence properties of single defects in diamond.** (a) **Structure of nitrogen-vacancy (NV) center and subsitutional nitrogen (N) defect centers in diamond.** (b) **Energy level diagram of the NV center showing spin polarization via crossover into the metastable excited state. (c) Electron spin resonance (ESR) for a single NV at room temperature.**

The energy level structure of the NV defect pertinent to our experiments is shown in Figure 8(b). Under optical excitation, the electron spin state is preserved. However, once in the optical excited state, it is possible for electron spin states other than m = 0 to spontaneously cross over into a meta-stable spin singlet. From here the excited electron eventually decays back to the ground state but only to the m = 0 state. As a result, the NV electron spin becomes polarized to a high degree (> 80%) after only a few optical pumping cycles, as illustrated in Figure 8(b). This spin polarization mechanism is very fast,[8] limited only by the decay rate of the metastable state which is on the order of 100 nsec.

In addition to spin polarizing the electron, the metastable excited state also provides spin-selective readout. This is because electrons initially in the m = +/- 1 ground spin state give a lower fluorescence emission rate, due to their being trapped in the non-fluorescing meta-stable excited state, than electrons initially in m = 0. This is

[7] Goss, J. P. et al. Comment on "Electronic structure of the N-V center in diamond: Theory". Physical Review B 56, 16031-16032 (1997).

[8] Jelezko, F., Gaebel, T., Popa, I., Gruber, A. & Wrachtrup, J. Observation of coherent oscillations in a single electron spin. Physical Review Letters 92, 076401 (2004).

shown in Figure 8(c).[9] Here the fluorescence of a single NV drops about 30% when the microwave field mixes the ground state electron spin sublevels.

Based on this data, it is possible to project whether or not single shot spin readout is possible at room temperature. For a single-shot readout fidelity of 95%, a signal to noise (SNR) ratio of about 10 is required. In the shot noise limit, this implies that 100 photons must be collected before the m = 0 state undergoes a spin flip. Since, it is estimated that up to 1000 fluorescent photons can be emitted before this happens, it appears that single-shot readout is possible in principle. However, in practice the fluorescence collection efficiency is typically about 2%, and hence single-shot readout can not currently be demonstrated. Nonetheless with improvements in fluorescence collection efficiency, for example using optical waveguides or cavities, room temperature single-shot spin readout of single NVs should be possible in the near future.

Having established that efficient initialization and readout of the NV is possible even at room temperature, we now consider how many quantum gates can be implemented before de-coherence effects dominate. Because, the NV has electron spins, it is possible to get relatively fast Rabi frequencies for single-qubit gates. An example is shown in Figure 9(a) where a 7 nsec Rabi frequency is observed on the electron spin transition for a single NV between the conductors of a co-planar microwave stripline. It is projected that Rabi frequencies up to a few nanoseconds are possible with better stripline design.

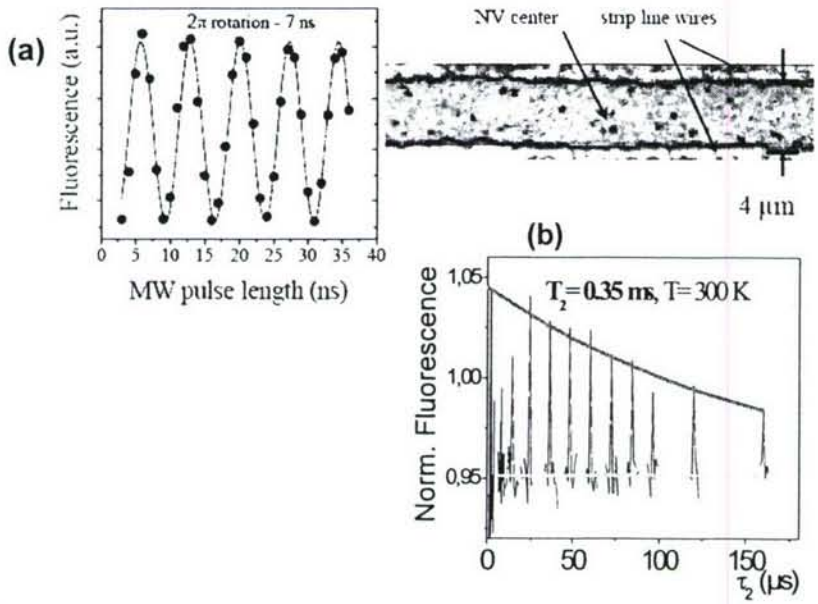


**Figure 9. (a) Fast Rabi flops of the electron spin on a single NV. The NV center was located between the conductors of a co-planar 50-Ohm stripline with a 4 micron gap. (b) Hahn echo decay curve of a single NV electron spin recorded at room temperature. During each echo sequence, $\tau_1$ was fixed and $\tau_2$ was varied. Decoherence leads to a reduction of echo amplitude for long time intervals between pulses. The orange curve is an exponential decay fit indicating a phase memory time of 350 microseconds. The grey line shows the fluorescence level corresponding to the full loss of initial polarization providing a base line for the decay curve.**

[9] Nizovtsev et al, Optics and Spectrosocopy, 94, 848, (2003)

Finally, there is the question of the NV electron spin lifetime at room temperature. Typically, electron spins have microsecond lifetimes in room temperature solids, and hence only a few qubit gates would be possible even with a microsecond Rabi frequency. However, the situation is surprisingly different in NV diamond for a combination of reasons. First, diamond has a very rigid lattice and therefore has a Debye temperature that is nearly an order of magnitude higher than other solids. Thus a room temperature diamond would be expected to have properties similar to other solids at 30 K. In practice, interaction with lattice phonons causes population relaxation on a time scale determined by the spin-lattice relaxation time $T_1$. A spin-lattice relaxation time of 1.2 ms at room temperature was reported from NV ensemble measurements.[10]

Second, the diamond host is almost spin-free, with only 1% abundant $^{13}C$. Thus, decoherence producing spin flip-flops are suppressed due to the large spacing between adjacent spins in the lattice. In practice, if any impurity spins are present in the lattice they might form a spin bath and cause the NV spin to decohere via spin-spin interactions. Such spin flip-flops related to nitrogen spins are confirmed to be the main cause of decoherence for NV centers[11] (single substitutional nitrogen is known to be the major paramagnetic impurity in synthetic diamonds). In fact, it was recently demonstrated that a single NV center electron spin can be made to decohere by coupling to an electron spin bath of nitrogen impurity spins.[12] In order to increase coherence time, the use of higher purity diamond crystals with lower concentration of nitrogen is essential. On the other hand, nitrogen is necessary for formation of NV defects. Auspiciously, NV centers can be created in ultrapure diamond by single ion implantation of nitrogen.[13] This novel technique does not require the presence of nitrogen in the diamond lattice and thus ultrapure (type IIa) diamond can be used as substrate.

The coherence time of such an implanted defect is shown in Figure 9Figure 8(b). The Hahn echo decay time of this single NV defect is 350 microseconds. This phase coherence time ($T_2$), is significantly longer than the previously reported 50 microseconds for NV ensembles in diamonds with very low nitrogen concentration. Presumably, in the present case coupling to $^{13}C$ nuclear spin limits the coherence time (natural abundance of $^{13}C$ is 1.1 percent). The homogeneous line-width of the $^{13}C$ spectrum is 100 Hz at room temperature indicating an average spin flip-flop time of 10 ms.[14] The electron spin feels a field jump if a pair of nuclei changes its mutual spin configuration. Flip-flop processes are strongly suppressed in close vicinity to NV center, because those nuclei experience a

---

[10] Redman, D. A., Brown, S., Sands, R. H. & Rand, S. C. Spin Dynamics and Electronic States of N-V Centers in Diamond by Epr and 4-Wave-Mixing Spectroscopy. Physical Review Letters 67, 3420-3423 (1991).

[11] Kennedy, T. A., Colton, J. S., Butler, J. E., Linares, R. C. & Doering, P. J. Long coherence times at 300 K for nitrogen-vacancy center spins in diamond grown by chemical vapor deposition. Applied Physics Letters 83, 4190-4192 (2003).

[12] Epstein., R. J., Mendoza., F. M., Kato., Y. K. & Awschalom, D. D. Anisotropic interactions of a single spin and dark-spin spectroscopy in diamond Nature physics 1, 94-98 (2005).

[13] Meijer, J. et al. Generation of single color centers by focused nitrogen implantation Applied Physics Letters 87, 261909 (2005); Rabeau, J. R. et al. Implantation of labeled single nitrogen vacancy centers in diamond using N-15. Applied Physics Letters 88, 023113 (2006).

[14] Hoch, M. J. R. & Reynhardt, E. C. Nuclear-Spin-Lattice Relaxation of Dilute Spins in Semiconducting Diamond. Physical Review B 37, 9222-9226 (1988).

strong hyperfine coupling induced energy shift with respect to the spin bath (frozen core effect). The decoupling radius $\delta$ is given by[15]

$$\delta = \left[ 2S \frac{\gamma_e}{\gamma_n} \right]^{1/4} a$$

(Here S is an electron spin quantum number, $\gamma_{e,n}$ are the gyromagnetic ratios of electron and nuclear spins and $a$ is the average nearest neighbour separation between nuclear spins). Substitution of $a$ = 0.44 nm for natural 1.1 % $^{13}C$ abundance yields the minimum radius of the frozen core to be 2.2 nm This corresponds to random jumps of the defect center ESR frequency by about 2.5 kHz, which is in agreement with the experimentally observed phase coherence time. Hence, the availability of isotopically pure diamonds might lead to further increase of $T_2$. In addition, the angular dependence of dipolar coupling can be used for the suppression of decoherence by applying an appropriate magnetic field.[16]

Regardless of future improvements in the room-temperature NV spin lifetime, the present value of 0.3 msec combined with the observed 7 nanosec Rabi frequency gives a projected ~50,000 single qubit operations per coherence time. Clearly, this is an unprecedented number for a room temperature solid state quantum computer.

[15] Khutsish.Gr. Spin Diffusion. Soviet Physics Uspekhi-Ussr 8, 743-& (1966)

[16] de Sousa, R. & Das Sarma, S. Theory of nuclear-induced spectral diffusion: Spin decoherence of phosphorus donors in Si and GaAs quantum dots. Physical Review B 68, 115322 (2003).

## 4. Two-qubit coupling of room temperature NVs

The long coherence times of engineered NV defects allows for relatively long-range coherent coupling among defects. For example, given a $T_2$ of 0.35 ms two electron spins (S=½) separated by up to 15 nm could be coherently coupled. Although single NV and N defects can be created one by one using an implantation technique, generation nanometer spaced pairs remains challenging. Two factors affect the positioning accuracy. The first is scattering of nitrogen ions in diamond during implantation (straggling). The second factor is ion beam focusing accuracy. Current technology allows implantation of single ions[17] but implantation accuracy is limited to 20 nm.[18] *Implanting nitrogen molecules* rather than atoms allows solving both problems (see Figure 10(a)). Although absolute positioning accuracy is still limited by the implanter focus, the *relative* distance (spacing between two defects) is only affected by straggling. Note that straggling can be minimized by decreasing the implantation energy (see Figure 10(b)). Relative positioning of defects with distances below 5nm was achieved by implantation of molecules with a kinetic energy of 14 keV.

After implanting two closely spaced nitrogen atoms using this molecular implantation techniques the sample was annealed to form NV centers. With the implantation conditions used it was found that only 1% of the molecular implants were converted to a NV-N pair, whilst the rest were left as unpaired NV. Due to the low conversion efficiency, no pairs of NV were observed. As a result, we have concentrated on the NV-N pairs. Evidence for NV-N coupling comes from level anticrossing and electron spin resonance experiments. Since the substitutional N defect is an electron spin ½ system, dipolar coupling between the two spins occurs. If the dipolar coupling is weak compared to the NV center zero-field splitting and Zeeman effect, perturbation theory can be applied to the description of magnetic interactions between the two defects. The Hamiltonian describing the coupled NV-N spin system is[19]

$$H = g_e \beta_e \hat{B} \hat{S}_1 + \hat{S}_1 \hat{D} \hat{S}_1 + g_e \beta_e \hat{B} \hat{S}_2 + \hat{S}_1 \hat{T} \hat{S}_2 \qquad (1)$$

where $\hat{S}_1, \hat{S}_2$ are spin matrices corresponding to NV and N spins, respectively, $\hat{D}$ is the fine structure tensor describing the interaction of the two uncoupled electron spins of the NV defect and $\hat{T}$ is the magnetic dipolar interaction tensor. Eigenenergies as a function of external B-field, shown in Figure 10(c), were obtained by diagonalising the spin Hamiltonian. Energy levels are identified according to individual defect spin quantum numbers. According to the energy level scheme, the splitting between doublet components corresponds to dipole-dipole coupling and is expected to be 14 MHz for a defect separation distance of 1.5 nm.

---

[17] Persaud, A. et al. Single ion implantation with scanning probe alignment. Journal of Vacuum Science & Technology B 22, 2992-2994 (2004).

[18] Jamieson, D. N. et al. Controlled shallow single-ion implantation in silicon using an active substrate for sub-20-keV ions. Applied Physics Letters 86, - (2005).

[19] Vanoort, E., Stroomer, P. & Glasbeek, M. Low-Field Optically Detected Magnetic-Resonance of a Coupled Triplet-Doublet Defect Pair in Diamond. Physical Review B 42, 8605-8608 (1990).

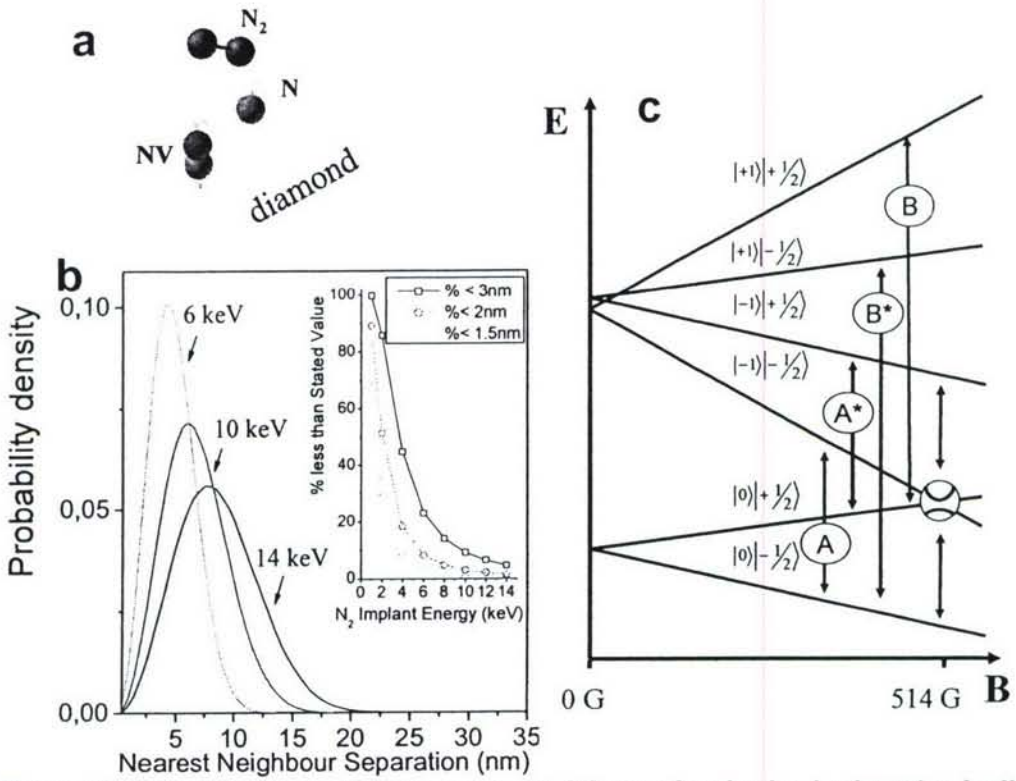


**Figure 10. Generation of coupled spin pairs. (a) Scheme of molecular implantation leading to formation of NV-N spin pairs. After implantation of single $N_2^+$ ions N-N pairs and vacancies (V) are generated in the diamond substrate. Annealing leads to conversion of such pairs into NV-N pairs. (b) Monte-Carlo simulation of single nitrogen ion paths in diamond (implantation energy 7 keV). After entering the diamond lattice, the chemical bond of $N_2^+$ molecule is broken and the two N penetrate independently in the diamond. Since both N atoms start at the same point, the average final separation between ions for 14 keV $N_2^+$ molecules corresponds to a spread of positioning of single N ion with 7 keV energy which is 3.6 nm according to STRIM calculations. (c) Energy levels of dipole-dipole coupled NV-N pair.**

A typical ESR spectrum of a single spin pair is shown in Figure 11(a). As compared to an uncoupled defect, the pairs show a line splitting into two sets of doublets. We find a level anti-crossing feature at $B_0$=514G indicating a coupled S=1, S=1/2 system. To demonstrate the coherent nature of the coupling electron spin echo modulation experiments were used. In the spin Hahn echo measurements ($\pi/2 - \tau - \pi - \tau - \pi/2$ – echo), the amplitude of the echo signal was measured as a function of the pulse separation $\tau$. The $\pi/2$ and $\pi$ pulses in both experiments were 15 and 30 ns, respectively. Therefore the bandwidth is larger than the splitting allowing full excitation of the EPR doublet (AA* transition shown in Figure 11(a)). The echo envelope shows periodic oscillation (ESEEM, electron spin echo modulation - Figure 11(b)). This modulation results from the coherent precession of the NV center spin in the field created by the nitrogen spin. The related phase acquired by the NV spin is not refocused by the echo sequence resulting in periodic oscillation of the echo amplitude. From a Fourier transformation of the oscillation pattern, the coupling frequency is obtained, yielding an energy splitting between sublevels equivalent to that observed in the EPR spectrum of

Figure 11(a). The Hahn echo modulation shows not only the frequency which corresponds to NV-N coupling, but also satellites corresponding to the internal hyperfine coupling associated with $^{14}N$. Since any static frequency difference between spins is refocused by the echo sequence, observation of the echo modulation pattern is an unambiguous demonstration of coherent coupling. It is important to note, that no decay of the echo is visible within the measurement time interval.

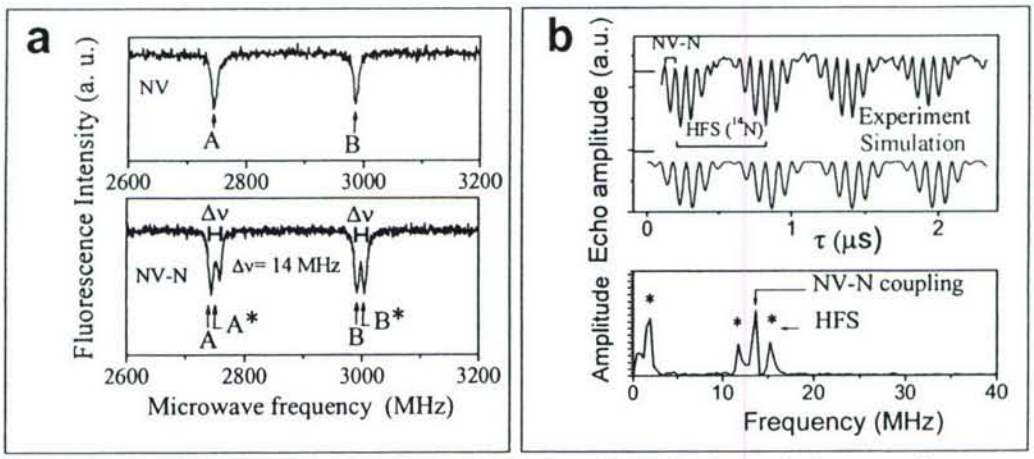


**Figure 11. Magnetic resonance on NV-N spin pairs. (a) Optically detected electron spin resonance spectrum of a single NV-N pair in weak magnetic field. The upper graph shows the ESR spectrum of a single NV center, indicating two transitions from $m_s$=0 to $m_s$=+/- 1 spin states (A and B). When dipolar coupling is present, each line splits into a doublet (A,A* and B,B* transition shown in the lower graph). (b) Hahn echo modulation and its Fourier transformation showing coupling between the two spins. Lower graph shows simulation of ESEEM pattern based on dipolar interactions between NV-N electron spins and hyperfine interaction with $^{14}N$ nucleus. Arrow marks coupling frequency between N and NV electron spins. Asterisks indicate frequencies associated with $^{14}N$ hyperfine structure.**

Only the NV center couples to the optical field and hence optical initialization can only be applied to the NV center. A symmetric shape of the ESR doublet in Figure 11(a) indicates that states $|0\rangle|+1/2\rangle$ and $|0\rangle|-1/2\rangle$ are populated equally under normal conditions. To polarize (i.e. initialize) the nitrogen spin, resonant spin flip-flop processes induced by dipolar coupling between the NV and N were exploited. Since the spin flip-flop is energy conserving, it is suppressed when the spins are not energetically equivalent, which occurs at low magnetic fields in the NV-N system (see Figure 12(a)). To achieve polarization transfer, the frequencies of NV and N spin transitions were tuned into mutual resonance by applying a magnetic field along the symmetry axis of the NV defect. Exact degeneracy is given at the point of level anti-crossing B=514 G (see Figure 10(c)). The lower graph of Figure 12(a) shows the evolution of the ESR spectra (transitions BB* in the energy level scheme presented in Figure 10(c)) as a function of applied magnetic field. When the resonance condition is reached, at 514±20 G in this sample, the optical pumping on the NV defect rapidly polarizes the N defect as well via spin flip-flops (transition between states $|0\rangle|+1/2\rangle$ and $|-1\rangle|-1/2\rangle$). This polarization of the N defect is observed by the disappearance of the high frequency component of the

ESR spectrum. The time scale for polarization is given by the coupling strength between NV and N (14 MHz) and the optical pumping rate.

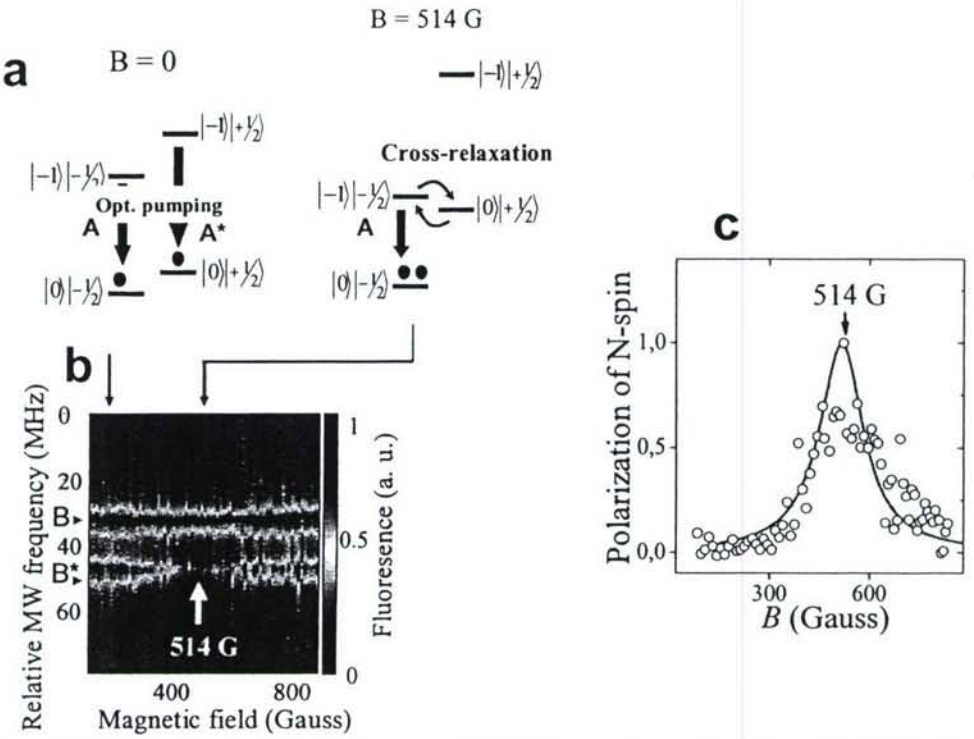


**Figure 12. Polarization transfer between coupled electron spins and build-up of polarization of 15N nuclear spin. (a) Evolution of ESR doublet BB* upon varying the external magnetic field. The upper graph represents the scheme of cross polarization of the N electron spin via dipolar coupling to the optically pumped NV center. (b) Polarization P of the N electron spin as a function of applied magnetic field. Polarization is defined as** $P = \frac{I_{B^*} - I_B}{I_{B^*} + I_B}$ **where** $I_{B^*}, I_B$ **are intensities of ESR spectrum components. The solid red line represents the model described in text. The upper graph shows the energy level scheme and rates, which were used to describe the build up of N electron spin polarization. (c) High resolution ESR spectra of NV-N pair (only transition B and B* are shown). Each transition shows hyperfine structure (transition 1 and 2 shown in inset) associated with $^{15}N$ nuclei. One of the hyperfine components is not visible at energetic resonance between NV and N electron spins (lower graph), indicating the build up of nuclear spin polarization of $^{15}N$ of NV center at NV-N resonance.**

The width of the polarization transfer resonance is expected to be limited by the homogeneous linewidth of both spin transitions, i.e. some kHz. However, under continuous optical illumination, the resonance of the NV center broadens because optical pumping disturbs the spin coherence: hence polarization transfer occurs over a wide magnetic field range because of the overlap between the tails of the resonance lines. To describe the build up of N polarization we have employed a model including dipolar coupling ($\Delta$), spin-lattice relaxation of nitrogen and NV spins ($\gamma_{SL}^{N}, \gamma_{SL}^{NV}$) and optical pumping acting on NV spins ($\gamma_{opt}^{NV}$). The mutual spin flip-flop rate was calculated as product of dipolar coupling ($\Delta$=13 MHz in the presented case) and the overlap integral $S$

between NV and N lineshapes[20] $S = 1\Big/\left[1+\frac{\Delta\cdot D}{2\left(\gamma^{N}\cdot\gamma^{NV}\cdot\gamma_{OPT}^{NV}\right)}\right]^{2}$. Here $\gamma^{N},\gamma^{NV}$ are the dark dephasing rates of N and NV spins, and $D$ is detuning between ESR lines, respectively. The result of calculation without any fitting parameters (the optical polarization and coherence time of the NV center was measured independently in pulsed ESR experiments) together with experimental data are shown in Figure 12(b).

Detailed examination of ESR spectra reveals not only disappearance of high frequency component of ESR doublet, but also asymmetric narrowing of spectral lines close to NV-N resonance (Figure 12(a)). This narrowing is related to build up of nuclear polarization of NV center. Each ESR line consist of two hyperfine transitions associated $^{15}$N nuclei. Those components are not well resolved in ODMR spectra presented in Figure 12(a) because of line broadening associated with optical pumping. Figure 12(c) shows ESR spectra recorded at low optical excitation power. The disappearance of one of the hyperfine transition indicates polarization of $^{15}$N nuclear spin close to NV-N resonance. Such polarization of the nuclear spins by optically oriented electron may arise from the "flip/flop" processes involving the simultaneous spin flip of a nucleus and electron spins.

The present results demonstrate a first step towards a controlled generation of a set of interacting spins *associated with* defects in diamond. Its potential usefulness for solid-state quantum information processing lies in the accessibility of long lived electron spin states by photons. Due to the point-like nature of the defect wave function, the spin coherence is very robust against external perturbations such that coherent control experiments can be carried out at room temperature. Given e.g. the value demonstrated in the present work, the coherence time exceeds the $2\pi$ rotation time by $10^4$. Potentially the present approach is thus well suited for quantum memory architectures, where the nitrogen defect nuclear spin would be the storage element. In the present work polarization of this nuclear spin via photons has been demonstrated. However, using standard methods of coherence transfer from electron to nuclear spins this can be converted to a memory architecture. Photons can be converted into an electron spin coherence of the NV center by EIT type techniques. From there coherence might be transferred to electron and subsequently nuclear spin coherence *of* the nitrogen impurity. Detuning *energy of* the two systems with respect to each other will result in photon storage in terms of nitrogen nuclear spin coherence.

---

[20] Abragam, A. Principles of nuclear magnetism (Claredon press, Oxford, 1961).

## 5. Control of NV optically excited states

Although it may be possible to build a room temperature solid-state quantum computer using NV diamond, scaling will be limited due to the fact that quantum coupling is possible only to nearby neighbors. This is because of the relatively fast $1/d^3$ roll off of the dipole-dipole coupling strength, where d is the distance between dipoles. To achieve coupling between arbitrary qubits in a large array, a photon mediated entanglement scheme is preferred.

Transfer of quantum information from photons to NV electron spins requires that spin-selective optical transitions be present. Since different laser polarizations do not spin-selectively excite NV optical transitions, the transitions must be spectrally resolved instead. For the NV center this happens at temperatures below about 10 K. However, as in most solids, there is a spectral spread in the optical transition frequencies of individual NVs owing to inhomogeneities in the local electric fields and strain. Therefore, the ability to tune the frequency of the spin-selective optical transitions of single NV centers is of crucial importance. Magnetic and electric fields are among the most prominent candidates that can be used for such control. Their influence on quantum states is well characterised and they can be conveniently controlled externally. Electric fields in particular allow for wide tuning of eigenstates and are hence popular control inputs. The electric field induced shift of the optical resonance lines has been observed for single atoms, ions in the gas phase[21] and single molecules[22] and quantum dots[23] or wells in solid state systems.[24] For color centers in diamond, only a few bulk studies on electric field induced spectral line shifts have been carried out.[25] Usually these studies are difficult because the magnitude of the Stark effect is on the order of the inhomogeneous linewidth. Moreover, ensemble averaging hides the individual Stark behaviors of the defects. Previous attempts to perform Stark shift studies on single NVs have been unsuccessful up to now. This is mostly related to the spectral diffusion which broadens the linewidths when the observation time exceeds the typical time interval between spectral jumps. Spectral bandwidths far exceeding the lifetime-limited (transform-limited) value were reported previously on NV centers.[26] It was suggested that spectral diffusion is generated by a fluctuating local electric field in the vicinity of the NV center, caused by ionization of optically active defects in diamond.

---

[21] Graeff, C. F. O. et al. Optical excitation of paramagnetic nitrogen in chemical vapor deposited diamond. Applied Physics Letters 69, 3215-3217 (1996).

[22] Brunel, C., Tamarat, P., Lounis, B., Woehl, J. C. & Orrit, M. Stark effect on single molecules of dibenzanthanthrene in a naphthalene crystal and in a n-hexadecane Shpol'skii matrix. Journal of Physical Chemistry A 103, 2429-2434 (1999).

[23] Empedocles, S. A. & Bawendi, M. G. Quantum-confined stark effect in single CdSe nanocrystallite quantum dots. Science 278, 2114-2117 (1997).

[24] Kador, L., Latychevskaia, T., Renn, A. & Wild, U. P. Radio-frequency Stark effect modulation of single-molecule lines. Journal of Luminescence 86, 189-194 (2000); Seufert, J. et al. Manipulating single quantum dot states in a lateral electric field. Physica E-Low-Dimensional Systems & Nanostructures 13, 147-150 (2002).

[25] Kaplyans.Aa, Kolyshki.Vi & Medvedev, V. N. Linear Stark Effect and Point Symmetry of N3 Center in Diamond. Soviet Physics Solid State,Ussr 12, 1193-& (1970).

[26] Jelezko, F. et al. Single spin states in a defect center resolved by optical spectroscopy. Applied Physics Letters 81, 2160-2162 (2002); Jelezko, F., Volkmer, A., Popa, I., Rebane, K. K. & Wrachtrup, J. Coherence length of photons from a single quantum system. Physical Review A 67, - (2003).

Here we demonstrate stable and lifetime limited optical excitation lines of single NV centers in diamond at low temperature. This key advance is achieved by careful selection of materials and sample preparation. We then took advantage of the high quality factor of the resulting optical resonances to investigate for the first time the Stark effect on single NV centers.

The NV defect in diamond is comprised of a substitutional nitrogen plus a vacancy in an adjacent lattice site. The defect belongs to the $C_{3v}$ symmetry group. It is usually described by a six electron model, where five electrons originate from the substitutional nitrogen and the dangling bonds of the unpaired carbon atoms. An additional electron is acquired from the diamond lattice making the defect overall negatively charged. The NV defect has an electron spin triplet ground state[27] S=1 with total symmetry $^3A_2$. The transition to the optically excited $^3E$ state ($\Delta E$=1.945eV) is a strongly allowed optical dipole transition[28] with a concomitant intense, red-shifted fluorescence related to emission into phonon sidebands. Single NV defect centers in a polished (100) type IIa diamond were investigated. The defects were imaged with a laboratory built low temperature confocal microscope. Defect excitation was carried out with a narrow band dye laser (Coherent 699-21) or a diode laser (New Focus, Velocity). The electric field was generated with 50 μm spaced electrodes. Electrodes were made by depositing 20nm of Mo and 200nm of Ag onto diamond at about 350 °C. A 400nm overcoat of $SiO_2$ was then deposited for insulation of the E-field from the He flow. For the experiments it turned out to be important to have Ohmic contact between the diamond and the electrode material. In the case of bad electrical contact, a pronounced transient Stark effect was found which was tentatively attributed to electrostatic screening effects caused by electrons in the bulk diamond material.

Figure 13(a) shows the fluorescence excitation line at the zero phonon transition frequency of a single defect center at T=2K. The line has a lorenzian shape with a linewidth of 13 MHz. Given an excited state lifetime for the NV center of 11.5 ns, the measured linewidth is determined by the time-energy uncertainty relation and corresponds to a high quality factor of a few $10^7$. Together with a remarkable spectral stability observed for some defects without any requirements for optical repumping, the excitation lines are well suited for investigation of the Stark effect at the single defect level.

The stable NV optical lines shown in Figure 13(a) can be used to achieve high-fidelity single-shot readout of the electron spin state. This is because the laser can be selectively tuned to the relevant electron spin transition. If there is no spectral diffusion, every attempt to resonantly excite the NV produces a detectable fluorescence burst. This is illustrated in Figure 13(b). Here, the NV is polarized into the m = 0 ground spin state and then read out by exciting with a laser tuned to the m = 0 optical transition frequency. If the fluorescent counts per burst is above a threshold, the readout is considered to be successful. As seen in Figure 13(b) a histogram generated by many repetitions of this readout experiment shows a bi-modal distribution with > 95% of the events falling into the successful readout category.

---

[27] Goss, J. P. et al. Comment on "Electronic structure of the N-V center in diamond: Theory". Physical Review B 56, 16031-16032 (1997).

[28] Davies, G. & Hamer, M. F. Optical Studies of 1.945 Ev Vibronic Band in Diamond. Proceedings of the Royal Society of London Series a-Mathematical Physical and Engineering Sciences 348, 285-298 (1976).

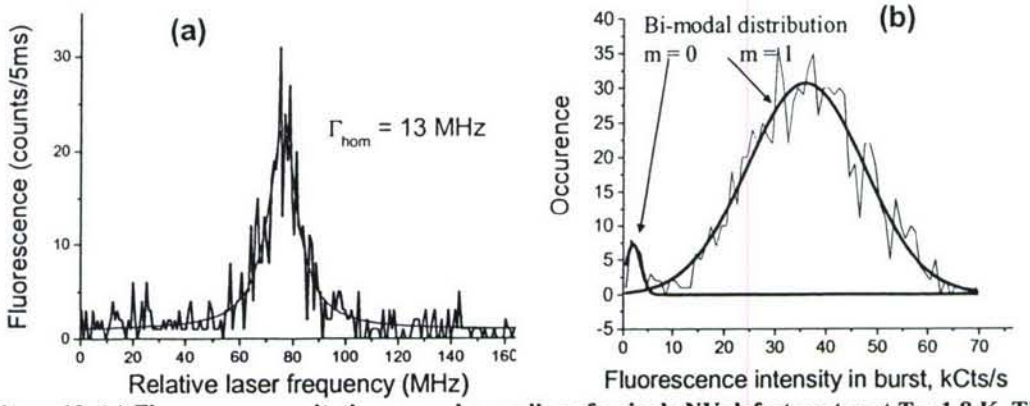


**Figure 13. (a) Fluorescence excitation zero phonon line of a single NV defect center at T = 1.8 K. This line, which was excited on resonance (637 nm) shows a lifetime-limited homogeneous width of 13 MHz. The excitation power was 5 nW, far below the saturation value of about 100 nW. (b) Demonstration of single shot spin readout of a single NV with > 95% fidelity. The NV was repeatedly prepared in the m = 0 ground state and then read out. Each time the number of counts per burst exceeded a threshold, the readout was considered successful.**

To second order in the local electric field **F** acting on the defect, the Stark shift of the electronic transition is given by

$$h\Delta\upsilon = -\Delta\boldsymbol{\mu}.\mathbf{F} - \frac{1}{2}\mathbf{F}.\Delta\boldsymbol{\alpha}.\mathbf{F}, \qquad (1)$$

where $\Delta\boldsymbol{\mu}$ and $\Delta\boldsymbol{\alpha}$ are respectively the dipole moment change and the change of polarisability tensor between excited and ground states. Higher order terms are expected to arise in eq. 1 via higher order hyperpolarisabilities.[29] However, estimation of the cubic term, related to the change in the second order polarizability $\chi^{(2)}$, indicates that it should be smaller than the quadratic term by a factor $F/F_{int}$, where $F_{int}$ is the internal field acting within the defect center. Since the applied electric fields range up to a few $MVm^{-1}$ in our measurements, third and higher order corrections are neglected in the Stark analysis. In order to extract the dipole moment and polarisability changes from the data, it is necessary to determine the value of the local field F from the externally applied E. Here we adopt the simplest approach using the Lorentz local field approximation $F = \frac{\varepsilon + 2}{3}E$, where $\varepsilon$ is the dielectric constant. With a value for $\varepsilon = 5.7$ for diamond this yields a local field enhancement factor of 2.6. The applied field is calculated by dividing the applied voltage by the distance between electrodes, together with a small correction factor of $2/\pi$ for the given electrode configuration (field at the center of two infinite half-plates).

Figure 14 shows a series of excitation spectra recorded while changing step wise the applied electric field from zero to 0.3 $MVm^{-1}$. The resulting spectral trails give an overview of the diversity of the Stark behaviors found for different individual defects. Inaccessible in ensemble measurements, the rich variation revealed here explains why little data on the Stark effect in diamond has been published so far. For electric fields up

[29] Shen, Y. R. The principles of nonlinear optics (Wiley, New York, 1984).

to a few $MVm^{-1}$, the Stark shift of the optical resonance is well fitted by linear and quadratic dependences, $\Delta\nu = aF+bF^2$. Comparing this expression to eq. (1) leads to the values of the dipole moment change and the polarizability change along the local field **F**, respectively named $\Delta\mu$ and $\Delta\alpha$. Figure 15 exemplifies three different cases of Stark behavior. Figure 15(a) describes a defect center showing a linear Stark effect with a = -6.3 $GHz/MVm^{-1}$ which corresponds to $\Delta\mu$ = 1.3 D (1 Debye = 3.33 $10^{-30}$ Cm). This value is very similar to values found in other cases, e.g. aromatic molecules in solid molecular hosts [Orr, Bru]. Most defect centers also show a quadratic electric field dependence. Figure 15(b) represents a defect with an almost exclusively quadratic component with $\Delta\alpha$ = -3.5 $10^4$ $Å^3$ and Figure 15(c) depicts a case where both a linear and a quadratic component are present. Here the polarizability change is $\Delta\alpha$ = -5.4 $10^4$ $Å^3$. Let us notice that we have used here the polarisability volume which is the polarisability divided by $4\pi\varepsilon_0$. (A statistical investigation of a few tens of single NV centers gave a distribution for $\Delta\mu$ between -1.5 D and +1.5 D. The values of $\Delta\alpha$ were found between -6 $10^4$ $Å^3$ and 0.)

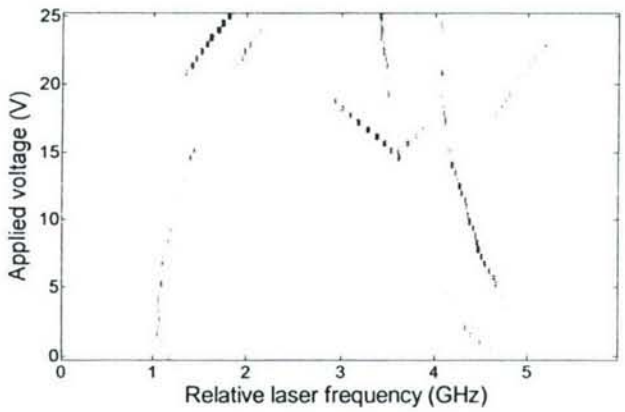


**Figure 14. Spectral trails of different single defects found in the same frequency scan. Excitation spectra have been recorded with step wise changes of the applied voltage from 0 to 25 V, corresponding to an applied field varying from 0 to 0.3 $MVm^{-1}$. These trails give an overview of the various individual Stark behaviours, hidden in ensemble measurements. Some excitation lines were observed only for a specific range of field values.**

The data of Figure 15 shows that it is possible to tune the NV optical transition by up to 10 GHz with an electric field on only about 1 MV/m. Diamond can withstand 100 times stronger electric fields and so it should be possible to easily span the 30 GHz wide inhomogeneous optical linewidth. Note that for impure diamonds, especially containing large amounts of nitrogen, the optical inhomogeneous width is more than 10 times wider. The problem is that the Stark shift is not always linear. To see why this is the case, a number of single NV centers were investigated and the results fitted to a model based on symmetry. The results are shown in Figure 16(b). Briefly, there are two orbital excited states. Both branches had never been observed before in a single NV. Figure 16(a) shows that the two branches have an anti-crossing near zero applied electric field. For zero electric field and zero strain, the two orbital branches are degenerate. However, this is usually not the case. Therefore when an electric field is applied it causes either a linear or quadratic shift depending on whether it produces a perturbation parallel or

perpendicular to that already present in the lattice. Note that electric field and strain are not distinguishable in this model so that in principle any strain can be exactly compensated by an electric field of the correct magnitude and orientation.

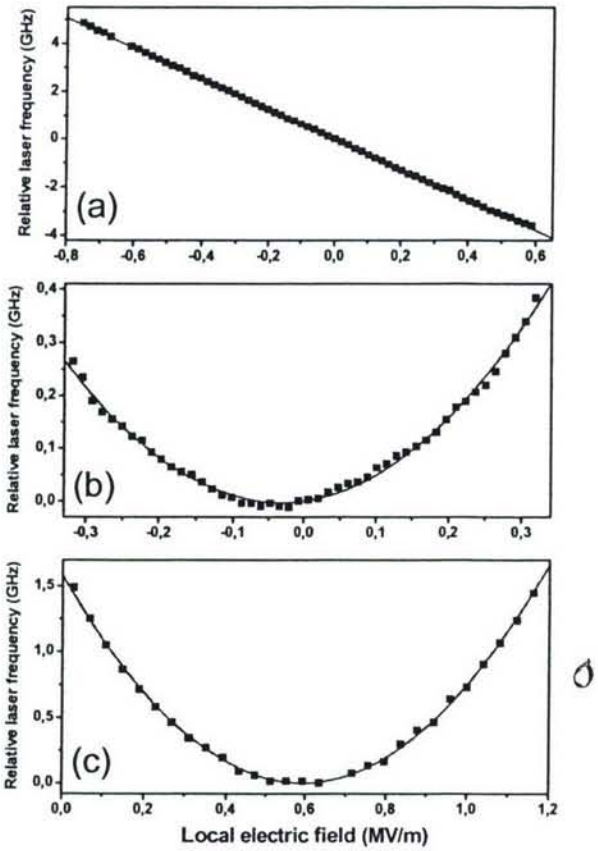


**Figure 15. Examples for the Stark shift of three different defect centers. The local electric field was calculated from the externally applied bias using the Lorentz local field correction (for details see text). (a) Linear Stark effect with $\Delta\mu$ = 1.3 D. (b) Mostly quadratic Stark effect with $\Delta\mu$ = -37 mD and $\Delta\alpha$ = -3.5 $10^4$ Å$^3$. (c) Linear and quadratic Stark dependences, with $\Delta\mu$ = 1.1 D and $\Delta\alpha$ = -5.4 $10^4$ Å$^3$.**

The model of Figure 16(b) is significant for another reason. One of the reasons that spin-based trapped ion quantum computers have been so successful is that it is possible to have state selective optical readout on one transition, and yet have optical Raman transitions on another to precisely manipulate the spins. It is natural to ask whether such a situation might exist in solids. As seen in Figure 16(b) this can indeed be the case for the NV. At certain electric field strengths, the spin sublevels in the lower branch of the optical excited state have anti-crossings. At these locations, optical Raman transitions become fully allowed and can be used to manipulate spins. At the same time, the upper branch remains a cycling transition and can be used for readout.

## 6. Summary

Several optically-addressed solid-state spin systems were studied to determine feasibility for use in scalable lattice-gas quantum computers. The rare earth doped oxides Pr and Eu showed the most early promise in the form of half minute coherence times with microsecond single-qubit gate operations, and long-range (~100 nm) two-qubit gates between nearby spins. However, nitrogen-vacancy (NV) diamond was eventually chosen. Surprising, it was found that NV diamond exhibited the key elements needed to develop few-qubit solid-state quantum processing nodes, even at room-temperature. These included the ability to optically initialize and readout the NV electron spin state, and ~50,000 single qubit operations per coherence time. We also demonstrated the relatively long distance (few nanometer) coupling of a single NV spin to the electron spin of a single substitutional nitrogen (N).

To achieve long range optical interconnections and entanglement between nodes, cryogenic cooling will still be required to sufficiently narrow the optical absorption lines. Due to inhomogeneous broadening in solids, this also requires stable, but tunable optical lines. We were able to demonstrate electric field tuning of the NV optical transition frequency, and we found diamond samples that exhibited exceptionally stable optical lines, and used these to demonstrate >95% fidelity for single-shot spin readout. We also mapped out the excited state energy level structure of the NV center and determined that is was possible to simultaneously have allowed optical Raman transitions on the lower optical branch and cycling transitions for spin readout on the upper branch. Together with a projected electron spin lifetime of minutes at low temperature, these are the key components needed to build a solid state version of a trapped ion quantum computer.